



Cite this: DOI: 10.1039/d5em00651a

## Speciation and leachability of zinc in energy-from-waste air pollution control residues and effects of partial neutralisation

Amitava Roy, <sup>a</sup> Dan Ting Chen, <sup>b</sup> Anna Bogush<sup>b</sup> and Julia A. Stegemann \*<sup>b</sup>

Seven UK air pollution control residues (APCRs) from municipal solid waste combustion were examined to understand the speciation of potentially ecotoxic zinc, before and after partial APCR neutralisation using acid wastes, as is sometimes conducted before disposal. Fe K-edge XAS showed Zn-containing magnetite (spinel) is an important phase in APCR, along with ferrihydrite. Linear combination fitting of X-ray absorption near edge structure (XANES) Zn K-edge spectra strongly concluded that the 2600–7300 mg kg<sup>-1</sup> of zinc in APCR is speciated mainly as spinel, hemimorphite, a glassy phase, zinc phosphate and hydrozincite, with statistically consistent findings both within and between APCR. The extended X-ray absorption fine structure (EXAFS) spectra of APCR mainly show the first Zn–O shell which is consistent with Zn in solid solution, glass and poorly crystalline phases. Presented in the context of a full review of previous studies, these results suggest changes in Zn speciation under modern operating regimes. pH-dependent leaching behaviour of the raw APCR was consistent with solubility control by secondary Zn(OH)<sub>2</sub> over the alkaline range, and also Zn<sub>5</sub>(OH)<sub>8</sub>Cl and hydrozincite at mid-alkaline pH. Partial neutralisation of the APCR with concentrated HCl formed secondary reaction products that agglomerated the APCR, but the same zinc species were found after neutralisation, and lower zinc leachability is attributable only to decreasing the pH to 10.0–10.7. Since this pH is unlikely to be stable in the environment (e.g., in interaction with landfill leachate at pH 5–8), industrial “treatment” by partial neutralisation does not reduce the environmental risk associated with zinc in APCR.

Received 20th August 2025

Accepted 1st May 2026

DOI: 10.1039/d5em00651a

rsc.li/espi

### Environmental significance

Air pollution control residues (APCRs) from waste-to-energy plants are hazardous wastes due to their high alkalinity and toxic element contents that are difficult to recover or treat for disposal. Industrial treatment with acid wastes neutralises their corrosivity before landfilling, but the common perception that this changes zinc speciation and leachability is unevidenced. Using advanced XAS and leaching tests, our results show that zinc occurs mainly as spinel, hemimorphite, glassy phases, zinc phosphate and hydrozincite in APCR, and these species persist after acid neutralisation, which does not alter their fundamental leachability. The evidence challenges the effectiveness of current practices and underscores the urgent need for a more sustainable approach to management of APCR.

## 1 Introduction

Generation of energy from waste (EfW) is a common way to recover value from municipal solid waste (MSW). Air pollution control residue (APCR) from MSW combustion represents only 2 to 6% of the original volume of the MSW. However, APCR are classified as hazardous waste in most jurisdictions (e.g., under European List of Wastes code 19 01 07\*; European Commission Decision 2000/532/EC) as they are alkaline (corrosive) and

contain high concentrations of toxic metals, such as zinc and lead, and soluble anions, such as chlorides and sulphates, and are difficult to recover or treat for disposal. One approach that has been applied industrially in the United Kingdom (UK) and elsewhere, is addition of acid wastes to APCR and blending with other neutralised wastes before landfilling. The main purpose of this treatment is to neutralise the corrosivity hazard but there is also an unevidenced conception that the agglomeration resulting from this treatment changes zinc speciation and leachability. The work reported here used X-ray absorption spectroscopy (XAS), a powerful technique for direct molecular-level study of specific elements at relatively low concentrations in complex materials, irrespective of their crystallinity, and pH-dependent leaching to gain a better understanding of

<sup>a</sup>Center for Advanced Microstructures & Devices, Louisiana State University, 6980 Jefferson Hwy, Baton Rouge, LA 70806, USA

<sup>b</sup>Centre for Resource Efficiency & the Environment (CREE), Department of Civil, Environmental & Geomatic Engineering (CEGE), University College London (UCL), Chadwick Building, Gower Street, London WC1E 6BT, UK. E-mail: j.stegemann@ucl.ac.uk; Tel: +44(0)207 679 7370



the zinc speciation in, and leachability from, APCR, before and after partial neutralisation.

## 2 Previous work

APCRs from MSW combustion are generated in the flue gas cleaning process, and comprise fly ash particles and scrubbing residues, often with excess hydrated lime ( $\text{Ca}(\text{OH})_2$ ). The overall composition and mineralogy of APCRs is fundamental to zinc speciation and has been addressed in a previous publication.<sup>1</sup>

The concentration and speciation of zinc in APCR depends on the type of waste combusted, its content of chlorine, sulphur and water, the amount of excess air, and temperatures and residence times in the various stages of combustion and pollution control. Theoretically, zinc present in MSW as a metal or oxide should be completely volatilised during combustion and deposited on the surface of fly ash particles as a chloride, and/or an oxide,<sup>1</sup> but in practice it tends to partition approximately equally between the APCR and the bottom ash.<sup>2</sup> This partitioning may result from reaction of zinc to form less volatile  $\text{Zn}_2\text{SiO}_4$  and  $\text{ZnAl}_2\text{O}_4$  (ref. 3) at MSW combustion flame temperatures ( $\approx 1200$  °C).<sup>4</sup> Zn in APCR has been shown to be more concentrated with unreacted lime in the smallest size fraction.<sup>5</sup> Specific minerals previously identified for zinc in MSW fly ash and APCR by instrumental methods and geochemical equilibrium modelling are shown in Table 1. Zinc chlorides, hydrated chlorides and oxides dominate previous findings, but most workers have suggested that contaminants, including zinc, are widely dispersed in the APCR, with various types of uptake by a variety of minerals and also glass. The only other previous XAS investigation of APCRs found that  $\text{K}_2\text{ZnCl}_4$  predominated, with the presence of hemimorphite ( $\text{Zn}_4\text{Si}_2\text{O}_7(\text{OH})_2 \cdot \text{H}_2\text{O}$ ), spinels ( $\text{ZnFe}_2\text{O}_4$ ,  $\text{ZnAl}_2\text{O}_4$ ), surface adsorbed zinc, and hydrozincite ( $\text{Zn}_5(\text{CO}_3)_2(\text{OH})_6$ ).<sup>6</sup>

The controlling mineral phases previously identified for zinc leachability above pH 7 have been shown in bold characters in Table 1. Zinc oxide and hydroxide were shown to control zinc concentrations in solution in the alkaline pH range typical of water leachates of APCR, though Eighmy, *et al.*<sup>7</sup> did conclude that leaching of zinc was controlled by  $\text{ZnCO}_3$ , and Astrup, *et al.*<sup>8</sup> and Wang, *et al.*<sup>9</sup> also found  $\text{Zn}_2\text{SiO}_4$  to control zinc leaching for some APCR. Interestingly, Zhang, *et al.*<sup>10</sup> found control of leaching in the neutral range by a zinc hydroxychloride,  $\text{Zn}_5(\text{OH})_8\text{Cl}_2$ , though ZnO dominated at higher pH.

Struis, *et al.*<sup>13</sup> found gahnite ( $\text{ZnAlO}_4$ ) to be an important Zn containing phase in a Swiss MSW fly ash, and Rissler and co-workers,<sup>6,21</sup> additionally found franklinite, with more of both spinels in APCRs from fluidised bed facilities than fly ash from grate combustion systems, in Sweden. Spinels have the general formula  $\text{A}^{2+}\text{B}_2^{3+}\text{O}_4$  (mostly cubic crystal structure), where the (tetrahedral) A site is usually occupied by divalent elements, such as  $\text{Mg}^{2+}$ ,  $\text{Fe}^{2+}$ ,  $\text{Zn}^{2+}$ , the (octahedral) B site is usually occupied by trivalent elements, such as  $\text{Al}^{3+}$ ,  $\text{Cr}^{3+}$ ,  $\text{Fe}^{3+}$ , and O can be O, S, Se, or similar anions.<sup>22</sup> There is extensive solid solution among the end members franklinite and gahnite at high temperatures, but immiscibility exists at lower temperatures.<sup>23,24</sup> The most common spinel is magnetite,  $\text{Fe}^{2+}\text{Fe}_2^{3+}\text{O}_4$ ,

which is found in many rocks and industrial by-products. Wei, *et al.*<sup>25</sup> reported magnetite, with various levels of substitution by Al and Ti, as an important phase in an MSW incineration bottom ash from Japan. Magnetite is found in fly ashes from coal-fired power plants, where it is mostly produced by the breakdown of pyrite in the coal during its firing.<sup>26,27</sup> Gomes, *et al.*<sup>28</sup> found that the magnetite in coal fly ash has a complex composition, with  $\text{Mg}^{2+}$  replacing  $\text{Fe}^{2+}$  and containing other minor elements such as Si. Magnetite is also found in other residues from thermal processing, including electric arc furnace dust<sup>29,30</sup> and non-ferrous smelter slags.<sup>31</sup> Manceau, *et al.*<sup>32</sup> found that Zn-containing magnetite is an important component of the contaminated soil around some historical smelters in France. As the spinel phase can be an important repository of zinc, special emphasis is placed on the magnetic fraction of APCRs in this investigation.

## 3 Materials & methods

### 3.1 Air pollution control residues

Seven APCR samples from six different UK EfW facilities, characterised in previous work,<sup>1</sup> were used in the work reported here. The samples are identified as A3 and A8 (both from the same source but sampled at different times), 1, 2, 4, 5, and 9. The concentration of zinc in these APCR samples ranged from 0.26 to 0.73%; average concentrations of major matrix elements determined by inductively coupled plasma optical emission or mass spectroscopy following aqua regia digestion are shown in Table 2.

### 3.2 Separation of magnetic material

To enable investigation of the relevance of magnetite to Zn speciation in APCRs, magnetic material was extracted from APCR sample A3 by dipping a plunger magnet into a suspension of ground ( $<63$   $\mu\text{m}$ ) APCR in water. Since magnetite is practically insoluble in pH 5 HCl at room temperature,<sup>33</sup> the collected material was acid-washed to separate magnetite from other agglomerated soluble phases before drying at 60 °C.

### 3.3 Partial neutralisation to target pH 9

To mimic the blending of APCR with waste acid practiced by industry, the pH of a 20 g subsample of each APCR was adjusted with a solution of analytical grade HCl at a liquid-to-solid (L/S) ratio of 1 L  $\text{kg}^{-1}$ . Between 6.0 and 10.5 meq  $\text{g}^{-1}$  of acid (depending on the APCR) were added gradually over a period of 4 h, to a target pH of 9. The samples continued to react after the 4 h acid addition period and the actual final pHs were higher than 9 (Fig. 8). For simplicity, the following text refers to the partially neutralised APCR samples by their target “pH 9”; the original APCR samples are identified as raw.

It is important to note that this was a pH adjustment process intended to approximate industrial practice, not a washing process. There was no separation of a liquid leachate phase, but the samples were substantially dried by the strong exotherm associated with the neutralisation reaction, leaving all elements



Table 1 Zinc mineral phases previously identified in fly ash (\*) and APCRs (+) from combustion of municipal solid waste<sup>a</sup>

	Zinc oxide (including zincite)	Calcium zincate	Hydrozincite	Smithsonite	Zinc chloride	Simonkolleite	Potassium tetrachlorozincate	Zinc bromide	Gordaitte	Zinc oxy-sulphate	Zinc sulphate	Wurtzite	Zincowoodwardite	Spinel	Gahnite	Zinc phosphate	Hemimorphite	Willemite	Zinc silicate	Zinc metal
Sample	ZnO	$\text{CaZn}_2(\text{OH})_6 \cdot 2\text{H}_2\text{O}$	$\text{Zn}_5(\text{CO}_3)_2(\text{OH})_6 \cdot x\text{H}_2\text{O}$	$\text{ZnCO}_3$	$\text{ZnCl}_2$	$(\text{OH})_8\text{Cl}_2$	$\text{K}_2\text{ZnCl}_4$	$\text{ZnBr}_2$	$\text{Cl} \cdot 6\text{H}_2\text{O}$	$(\text{SO}_4)_2$	$x\text{H}_2\text{O}$	ZnS	$\text{Zn}_{0.625}\text{Fe}_{0.188}\text{S}_{0.188}$	$\text{Ni}_3\text{Fe}_2\text{O}_4$	$\text{ZnAl}_2\text{O}_4$	$(\text{PO}_4)_2$	$(\text{OH})_2 \cdot 2\text{H}_2\text{O}$	$\text{SiO}_4$	$\text{Zn}_2\text{SiO}_4$	Zn
7*	X			W	X		X	X	X		W			X*			X			X
11					X*															X**
12*	X																			
13*					X**	X						X			X					
14	X <sup>+</sup>											X**		X**	X*					
8 <sup>+</sup>	W		W																	W
10 <sup>+</sup>	W					W														
15 <sup>+</sup>	W																			W
16 <sup>+</sup>	X				X															
17 <sup>+</sup>			X		X						X									
18*	W							W												
19 <sup>+</sup>							X					X								
9 <sup>+</sup>	W																			X
20 <sup>+</sup>	X				X					X										W
6			X**				X**							X**		X**				X**

<sup>a</sup> X indicates phase identified in unaltered APCR; W indicates phase identified in hydrated APCR.

**Table 2** Average major element concentrations in the seven samples of air pollution control residue investigated in this study (% of total dry mass)<sup>1</sup>

Al	Ca	Fe	K	Mg	Na	P	Pb	Si	Ti	Zn	Cl	S
1.4	26	0.69	3.0	0.60	3.0	0.42	0.16	0.54	0.14	0.64	18	1.4

and species (apart from the evaporated water) associated with the solid “pH 9” APCRs.

### 3.4 pH-dependent leaching

Water leaching of Zn from the raw APCRs and “pH 9” APCRs A3, 4 and 5 was tested according to BS EN 12457-2:2002,<sup>34</sup> using MilliQ water at  $L/S = 10 \text{ L kg}^{-1}$  without pH adjustment. The contact time was extended to 48 h for comparability with the pH dependent leaching. pH dependent leaching of the raw APCRs was determined using DD CEN/TS 15364:2006,<sup>35</sup> with different additions of analytical grade  $\text{HNO}_3$ , also at  $L/S = 10 \text{ L kg}^{-1}$ .

Parameters of interest were analysed in all water leachates, all leachates over the full pH range for raw APCR A3, and the three leachates with pH values closest to pH 4, pH 7 and pH 10 for the other raw APCRs. Leachates were preserved to  $\text{pH} < 2$  with  $\text{HNO}_3$  and analysed by inductively coupled plasma optical emission spectrometry/mass spectrometry (ICP OES/MS); anions in water leachates were determined by ion chromatography. Leached solids from were dried at  $60 \text{ }^\circ\text{C}$  for mineralogical characterisation and are further referred to as leached APCRs.

The pH, Eh, anion and cation concentrations determined in the leachates were used in chemical equilibrium calculations using the software PHREEQC.<sup>36</sup> Saturation indices were calculated for candidate minerals that might control Zn concentrations in the leachates at six different pH values for raw APCR A3. Thermodynamic data for ZnO,  $\text{Zn}(\text{OH})_2$ ,  $\text{Zn}_2(\text{OH})_3\text{Cl}$ ,  $\text{Zn}_5(\text{OH})_8\text{Cl}$  and  $\text{ZnCO}_3 \cdot \text{H}_2\text{O}$  were from the WATEQ4F database; data for  $\text{ZnFe}_2\text{O}_4$  were reported by and for  $\text{Zn}_5(\text{CO}_3)_2(\text{OH})_6$  by Preis and Gamsjäger.<sup>37</sup> Saturation indices could not be included for Zn in glass or solid solution (e.g., in apatite or other spinels). The Davies equation was used to calculate activity coefficients in the high ionic strength leachates (i.e., total dissolved solids concentration of  $13\text{--}40 \text{ g L}^{-1}$ ). Minerals with saturation indices from  $-1$  to  $+1$  were considered to be the potential solubility controlling minerals.

### 3.5 X-ray absorption spectroscopy

X-ray absorption near edge structure (XANES) and extended X-ray absorption fine structure (EXAFS) spectroscopic analysis for Fe and Zn in all raw APCRs, the magnetic fraction of APCR A3, and Zn in “pH 9” APCRs 1, 8 and 9, and leached APCRs A3 and 9, was performed at Louisiana State University’s synchrotron research facility, the J. Bennett Johnston, Sr, Center for Advanced Microstructures and Devices (CAMD), USA.<sup>38</sup> XANES spectra were measured for five different subsamples of APCR A3 to get a better understanding of the micro-scale variability of speciation in the APCR.

CAMD is a second-generation electron storage ring source operating at 1.3 GeV. Zn K-edge measurements were conducted at the High energy X-ray Absorption Spectroscopy (HEXAS) (4.5–25 keV) and Wavelength Shifter Double Crystal Monochromator (WDCM) beamlines (7–18 keV), located on an 11-pole wiggler and a 1-pole wavelength shifter, respectively, that use water-cooled double crystal monochromators.<sup>38</sup> The Hexas monochromator has a pair of Ge 220 crystals, while the WDCM monochromator has a channel-cut Si 111 crystal. The beam dimension was 1 mm (height)  $\times$  10 mm (width). The monochromators were calibrated at 7112.0 eV and 9659.0 eV with the K absorption edges of Fe and Zn foils, respectively. Most XAS (combined XANES and EXAFS) scan at CAMD consisted of (with respect to the absorption edge): 5 eV steps from  $-200 \text{ eV}$  to  $-30 \text{ eV}$ , 0.25 eV (0.3 eV for Zn) steps from  $-30 \text{ eV}$  to  $30 \text{ eV}$ , 1 eV steps from  $30 \text{ eV}$  to  $100 \text{ eV}$ , and 0.05k (wavenumber) steps from  $100 \text{ eV}$  to  $12.0\text{k}$  ( $7655 \text{ eV}$  for Fe and  $10\,202 \text{ eV}$  for Zn). The acquisition time was 3–5 s depending on the concentration for each scan and at least three scans were acquired to obtain a good signal to noise ratio. A standard foil was always maintained between the 2nd and 3rd ionization chambers.

Given the indications in the literature of the relevance of spinels to Zn speciation in materials of this kind, the speciation of Fe in the APCRs was assessed by comparing their Fe K-edge XANES and EXAFS spectra with those of spinel reference materials: magnetite, franklinite ( $\text{ZnFe}_2\text{O}_4$ ) and  $\text{NiZnFeO}_4$ , and also ferrihydrite.

The speciation of Zn in the APCRs was assessed by comparing their Zn K-edge XANES and EXAFS spectra with those of Zn reference materials. Based on previous findings (Table 1), the reference materials selected for the experiments at CAMD were: ZnO (zincite),  $\text{Zn}(\text{OH})_2$ ,  $\text{Zn}_5(\text{CO}_3)_2(\text{OH})_6$  (hydrozincite, Avocado Research Chemicals Ltd A14590),  $\text{ZnCO}_3$  (smithsonite),  $\text{ZnCl}_2$ ,  $\text{ZnSO}_4 \cdot 7\text{H}_2\text{O}$ ,  $\text{Zn}_3(\text{PO}_4)_2 \cdot \text{H}_2\text{O}$  (hopeite),  $\text{ZnAl}_2\text{O}_4$  (gahnite),  $\text{ZnFe}_2\text{O}_4$  (franklinite),  $\text{Zn}_2\text{SiO}_4$  (willemite),  $\text{Zn}_4\text{Si}_2\text{O}_7(\text{OH})_2 \cdot \text{H}_2\text{O}$  (hemimorphite) and a reference glass containing  $7870 \text{ mg kg}^{-1}$  of Zn (Corning Glass IR-X, Smithsonian NMNH 117085) and Zn foil. Zinc chloride hydroxide (confirmed by X-ray diffraction [XRD] as simonkolleite;  $\text{Zn}_5(\text{OH})_8\text{Cl}_2 \cdot \text{H}_2\text{O}$ ) was synthesised in the laboratory by adding 10 g of  $\text{ZnCl}_2$  to 50 mL of MilliQ water, heating to  $80 \text{ }^\circ\text{C}$ , adding 0.59 g of ZnO nanopowder, aging for 24 h at  $80 \text{ }^\circ\text{C}$ , washing with acetone and drying at room temperature. Reference materials were measured in transmission and the APCR samples in fluorescence.

Three software packages, Athena in Demeter, Larch, and SixPack were used for principal component analysis (PCA), linear combination fitting (LCF), and target transformation.<sup>39–41</sup> PCA was performed over the range 9640 to 9760 eV. The spectra were decomposed into orthogonal principal components, each associated with an eigenvalue representing the variance explained by that component, where both eigenvalue and variance represent the amount of spectral variation captured by each principal component. Components with higher eigenvalue and variance explain more of the dataset’s structure and are therefore more significant. The number of significant components was determined using Malinowski’s factor indicator



function (IND).<sup>42,43</sup> LCF was performed with Athena over the range  $-20$  to  $30$  eV around the absorption edge. The combinatorial option was used for LCF, including all the phases with reasonable SPOIL values from target transformation, in which SPOIL is a target transformation metric quantifying the mismatch between the reconstructed and experimental spectra.<sup>42–44</sup>

To gain insight into the Zn coordination environment, curve fitting was used to fit theoretical spectra of Zn standards (*i.e.*, ZnO and ZnCl<sub>2</sub>) to the experimental Zn spectra of APCR A3 and APCR A8 pH 9.57, as representative samples, by adjusting EXAFS variables, including the coordination number  $N$ , interatomic distance shift  $\Delta R$ , energy shift  $\Delta E_0$ , amplitude reduction factor  $S_0^2$ , and mean-square disorder of neighbour distance  $\sigma^2$  ( $\text{\AA}^2 \times 10^{-3}$ ).

### 3.6 X-ray fluorescence

X-ray fluorescence (XRF) spectra of APCR A3 and its magnetic fraction were obtained at CAMD at the end of an XAS run, at  $10\ 211$  eV, for 200 seconds, using the same silicon drift detector. Since the spectra were collected in air, the low-Z elements below Ar were not observed. The spectra were normalized to the argon peak (from air, 1.28% by weight).<sup>45</sup> Since the experimental parameters were identical between measurements, they could be used for semi-quantitative analysis.

## 4 Results

### 4.1 Magnetic fraction of air pollution control residues

Application of the plunger magnet to the aqueous suspension of APCR A3 followed by acid washing collected about 3% of the total amount of APCR. This magnetic fraction is denoted MF in figures and related discussion. If all the iron in A3 were speciated as magnetite, this would only be  $\sim 1\%$  of A3; therefore, MF clearly contains other materials, with quartz, hematite, and amorphous materials prominent in the XRD pattern (Fig. A1, SI Appendix A).

The Fe K-edge XANES spectrum of MF is shown in Fig. 1a, for comparison with the spectra of the spinel reference materials. The pre-edge peak intensity (along AA') depends on the amount of divalent iron in tetrahedral coordination. The intensity is low in franklinite and higher in other spinels, including MF. The relatively high energy of the MF absorption edge indicates that much of the Fe is oxidised (ferric), *i.e.*, that many of the tetrahedral spinel sites are filled by divalent cations other than iron, *e.g.*, Mg, Mn, Cu, Ni, as well as Zn. The white line, along BB', is much sharper in franklinite than in magnetite. The peak intensities beyond the white line (BB') seem to be directly proportional to the atomic number of the cation, being higher for Zn and Ni. For example, the peak along the line CC' is present in the spectra of franklinite and nickel–zinc spinel but absent in that of magnetite. Given the large number of elements, at different concentrations in APCR, that can potentially substitute for Fe in spinels, the likelihood of finding a spinel reference material with a spectrum that exactly matches that of MF is low. The Fe K-edge spectrum for MF can be

considered to represent an “APCR spinel”, which is more similar to magnetite than franklinite or the nickel–zinc spinel. Of course, compositional differences within and among APCRs will yield a range of slightly different spinels.

The Fe K-edge EXAFS spectra of the APCR spinel (MF) and the magnetite reference material are shown in Fig. 1b. Though peak locations are very similar, their amplitudes are weaker for MF than for magnetite. This is also seen in  $k$  space (Fig. 1c). The Fourier transforms of these spectra (Fig. 1d) are all similar, having two shells corresponding to the Fe–O and Fe–(Fe, Zn) distances. The peak for the second shell in MF has a lower amplitude compared to the magnetite reference material. This may be due to higher disorder in the crystallites (Debye–Waller factor) or lower coordination, or both, indicating that MF is poorly crystalline.

The XRF spectra of APCR A3 and its magnetic fraction (MF) are shown in Fig. 2. Semi-quantitative analysis indicates that Fe is enriched by a factor of 57, and Zn by a factor of 1.7, in MF relative to the raw APCR. Cu, Ti, Ni, Mn and Cr are also enriched in MF (by factors of 4, 6, 36, 17 and 15, respectively).

### 4.2 Iron speciation in air pollution control residues

The Fe K-edge XANES and EXAFS spectra of the raw APCRs are shown in Fig. 3a, c and d. In Fig. 3a, Fe K-edge XANES spectra of the raw APCRs are characterized by a weak pre-edge peak (along AA'), very similar white line shape, intensity and location (along BB'), and a weak bulge at higher energy (CC'). The spectra are very similar; any differences are due to the proportions of different Fe-bearing phases. In Fig. 3c, Fe K-edge EXAFS spectra of the raw APCRs are dominated by one single sinusoidal oscillation with similar frequencies and amplitude. This feature corresponding to only one dominant peak centred at approximately  $1.35$  Å, with comparable intensities in their Fourier transform spectra (Fig. 3d).

PCA of the XANES spectra indicates that two components justify more than 99% of the variation, and target transformation suggests that ferrihydrite and magnetite are indeed present in these samples (Fig. A2, SI Appendix A). The IND value from PCA corroborates this observation (Fig. A2c, SI Appendix A). A better fit was obtained by using the APCR spinel (MF) spectrum instead of the magnetite reference spectrum. LCF results for the XANES spectra for different APCRs with these two components indicate that Fe may be fully taken up in either ferrihydrite or spinel, or divided between the two (Table 3); it is probable that the proportions of ferrihydrite and spinel vary within, as well as between, APCRs. Fig. 3b illustrates the excellence of the LCF fit.

### 4.3 Zinc speciation in air pollution control residues

Fig. 4a shows the zinc K-edge XANES spectra of raw APCR A3, MF, and franklinite. Franklinite is the relevant end member for Zn solid solution in spinel, and has a much higher concentration of Zn (26% by mass) than MF (maximum 6% by mass, if Zn were not also present in other species). Zn K-edge XANES spectra of spinels from an industrial hazardous waste incinerator ash melting slag (1.8% Zn) and a Class C coal fly ash



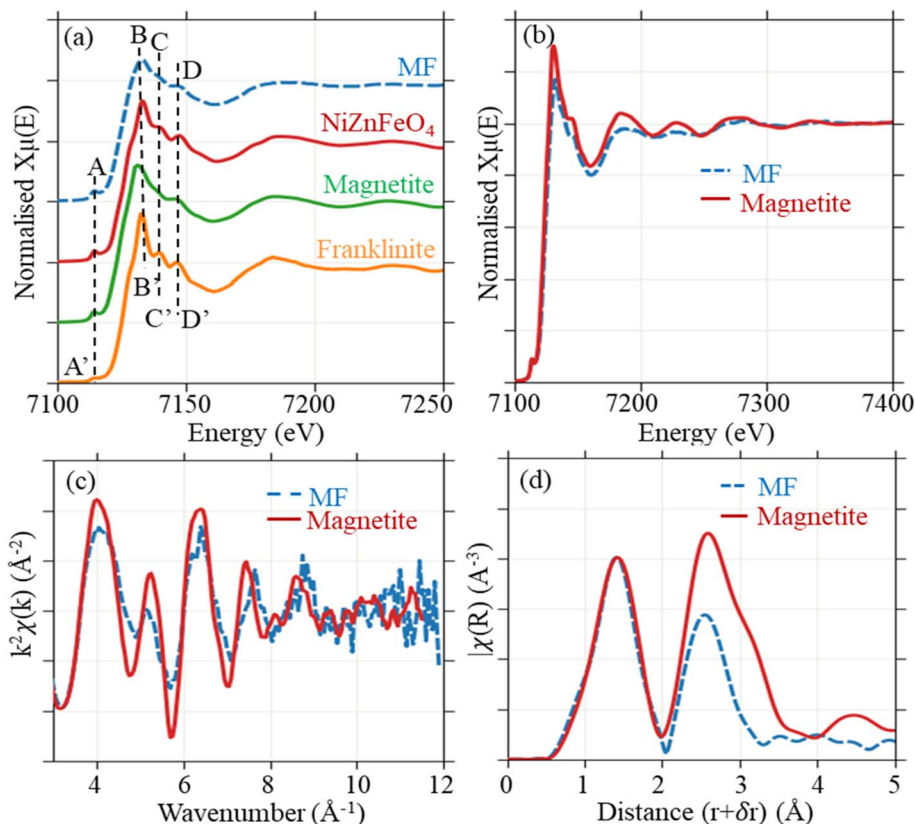


Fig. 1 (a) Fe K-edge XANES spectra of the magnetic fraction of APCR A3 (MF) and some standard spinels; (b) Fe K-edge EXAFS spectra of MF and the magnetite reference material, also (c) in  $k$  space; and (d) in Fourier transform of the EXAFS spectra (uncorrected for phase shift), with an interval  $k = 3\text{--}12 \text{ \AA}^{-1}$  and a Hanning window.

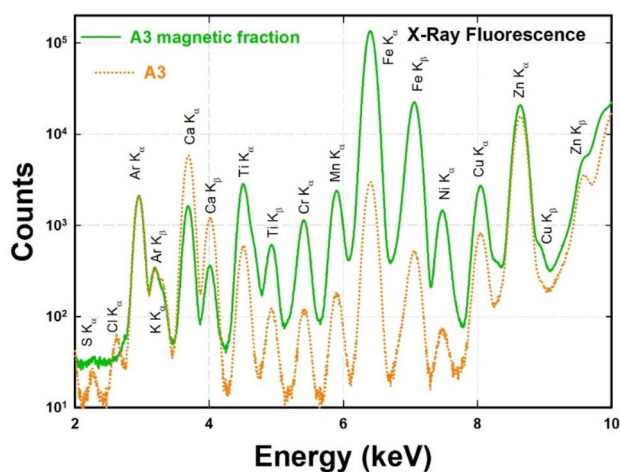


Fig. 2 X-ray fluorescence spectra of APCR A3 and its magnetic fraction (MF).

(0.013% Zn) are also included for comparison. The Zn spectrum for franklinite has a broad white line consisting of multiple weaker peaks. That of gahnite ( $\text{ZnAl}_2\text{O}_4$ ) (not shown) is similar, but the weaker peaks are at different energies and of different intensities. The Zn spectra of the spinels from the coal fly ash and the industrial slag have different white line structures,

possibly depending on zinc concentration. The Zn spectrum of MF has a broad white line similar to that of franklinite, but the smaller peaks have different intensities at different energies. The Zn EXAFS oscillations their Fourier transforms are shown in Fig. 4b and c, respectively. Only one oscillation is dominant for Zn in the raw APCR while multiple oscillations can be seen for Zn in MF and franklinite in  $k$  space. This resemblance is also evident in the Fourier transforms where two shells are seen for MF (and the industrial slag coal fly ash), at similar distances as for franklinite.

Fig. 5a shows the Zn K-edge XANES spectra of the raw APCRs. The K-edge absorption energy spreads over a narrow range from 9662.02 eV to 9662.67 eV, and the white line position changes slightly from 9667.62 eV to 9668.62 eV. The white line appears broad in some (APCR 2) while it is slightly sharper in others (APCR A3). The differences among the spectra apparent along the lines AA', BB' and CC' must be due to the proportions of different zinc-bearing phases in the raw APCRs. In Fig. 5b, the Zn K-edge APCR EXAFS spectra also appear broadly similar to each other in  $k$  space; minor differences can be observed at wavenumbers marked by the lines DD', EE', FF', and GG', which again relate to the contributions made by different phases. In Fig. 5c, the Fourier transform of Zn K-edge APCR EXAFS spectra all present one dominant peak at a distance of around 1.5 Å.



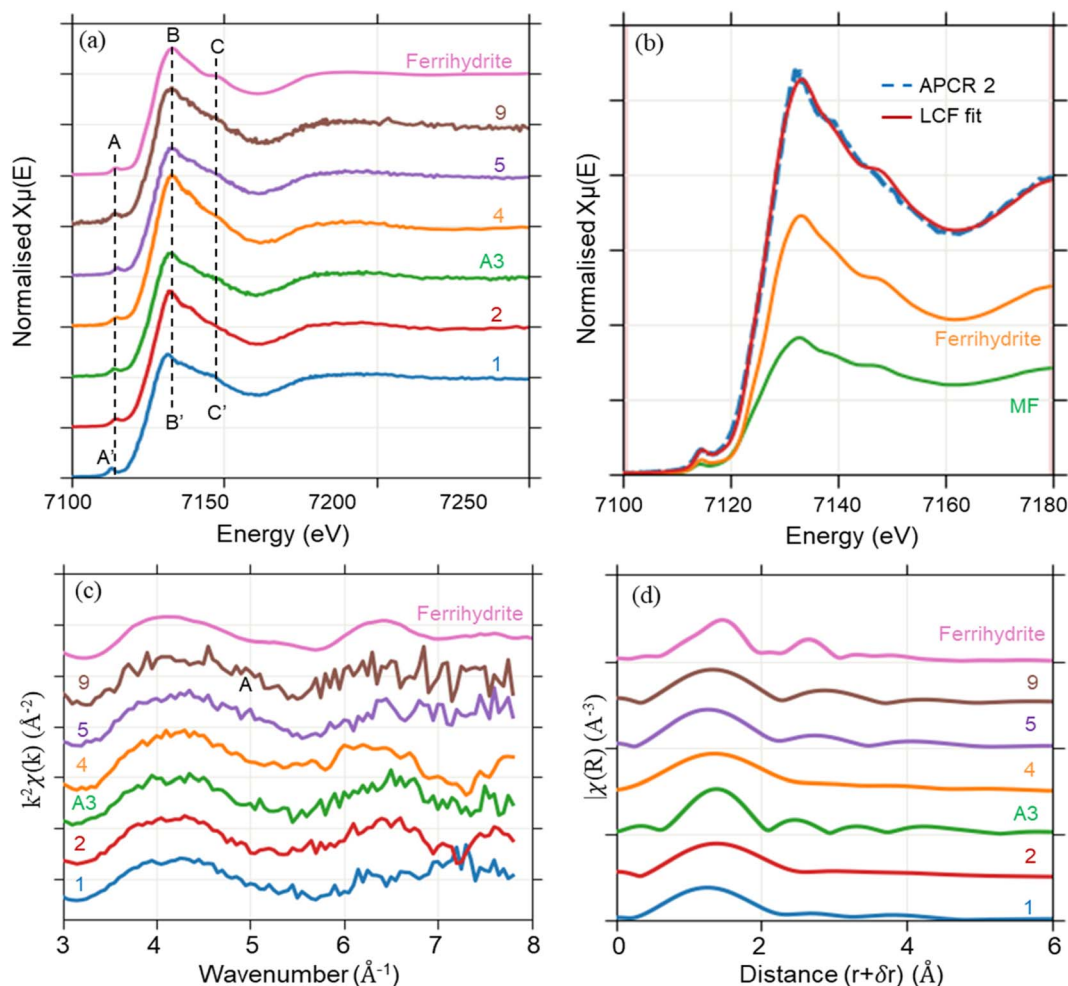


Fig. 3 (a) Fe K-edge XANES spectra of raw APCRs and ferrihydrite; (b) linear combination fitting of Fe K-edge XANES spectrum of APCR 2; (c) Fe K-edge EXAFS spectra of raw APCRs and ferrihydrite; and (d) Fourier transform of the EXAFS spectra (uncorrected for phase shift), with an interval  $k = 3\text{--}7 \text{ \AA}^{-1}$  and a Hanning window.

Table 3 Proportions of ferrihydrite and magnetite determined by linear combination fitting of raw APCR Fe K-edge XANES spectra

APCR	Ferrihydrite	APCR spinel (MF)	R-Factor
1	0.13	0.87	0.0040
2	0.69	0.31	0.0018
A3	0.52	0.48	0.0012
4	1.00	0.00	0.0030
5	0.00	1.00	0.0052
9	0.62	0.38	0.0020
Average	0.49	0.51	

Based on the Zn K-edge XANES spectra of the APCRs and reference materials, PCA was first used to determine that there appear to be three significant phases present in the raw APCRs (Table 4). Target transformation analysis was then used to determine the phases likely to be present (Table 5). The SPOIL value for the spectrum MF, the spinel from APCR A3, is lower than that of the franklinite reference materials, which reveals

the similarity among the spinels in the APCRs.  $\text{ZnCl}_2$  has the lowest SPOIL value, but the Zn K-edge EXAFS spectra (Fig. 5b) are dominated by a single strong oscillation, which matches the Zn–O shell in Corning Glass IR-X or  $\text{Zn}_3(\text{PO}_4)_2 \cdot x\text{H}_2\text{O}$  better than the Zn–Cl shell in  $\text{ZnCl}_2$ , so  $\text{ZnCl}_2$  can be present in only a very minor amount. This is supported by the distance of the first peak in the Fourier transform of APCR A3, which is close to that of hydrozincite (Zn–O) and much shorter than that of zinc chloride (Zn–Cl) (Fig. 5d).

LCF for the Zn K-edge XANES spectra was then performed to estimate the proportions of the potential zinc-containing phases present in the APCRs. The LCF results in Table 6 include the spectra measured for five subsamples of A3 (Fig. A3, SI Appendix A); A3i is the sample referred to elsewhere in this paper. Fig. 5b and c show the convincing fits for the two APCRs with the lowest (APCR A8) and highest (APCR 2) R-factors. The sum EXAFS spectra based on the proportions determined by LCF (Table 6) confirm good fit (e.g., for APCRs A8 and 2, in Fig. A4, SI Appendix A). As illustrated in Fig. 6 for hydrozincite, linear normal probability plots for each of the identified



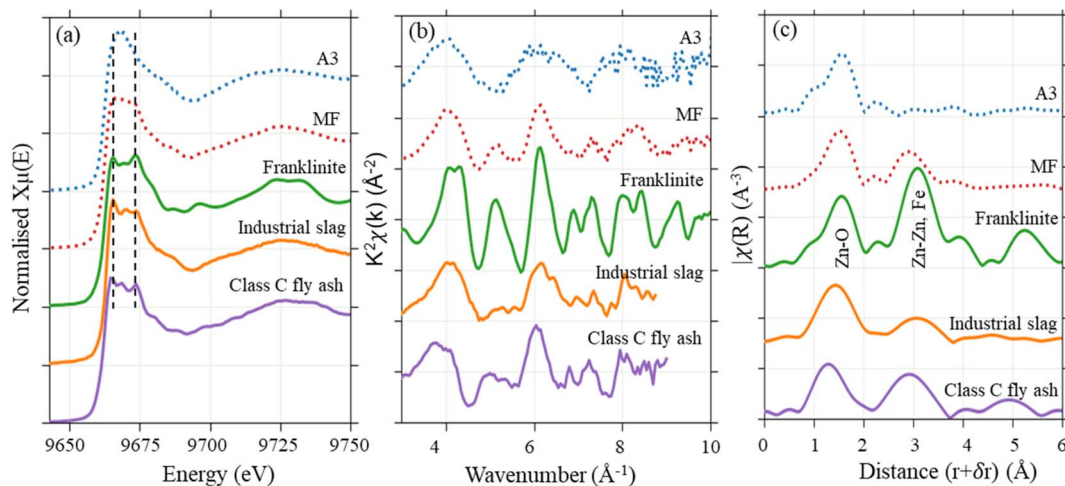


Fig. 4 (a) Zinc K-edge XANES spectra of raw APCR A3 and its magnetic fraction (MF) along with those of franklinite, an industrial slag and Class C fly ash; (b) EXAFS in  $k$  space of the same samples; (c) their Fourier transforms.

mineral phases indicate that all of the APCR samples and subsamples belong to the same population (Fig. A5, SI Appendix A). The different mineral proportions determined by LCF are thus a consequence of microscale APCR heterogeneity rather than real differences between the APCRs.

Curve fitting to theoretical standard was performed to fit theoretical spectra (*i.e.*, ZnO with tetrahedral Zn–O and ZnCl<sub>2</sub>

with tetrahedral Zn–Cl), respectively, to the experimental one of raw APCR A3, shown in Fig. A6 and A7, SI Appendix A. The same fitting was conducted to the experimental spectra of ZnO and ZnCl<sub>2</sub>, shown in Fig. A8 and A9, SI Appendix A. The best fit results (Table A1 and Fig. A6a, b, SI Appendix A) show that the first shell of APCR A3 was obtained with a coordination number of 4.1 at a distance of 1.943 Å ( $S_0^2 = 0.93$ ;  $E_0 = 0.21$  eV;  $\Delta R =$

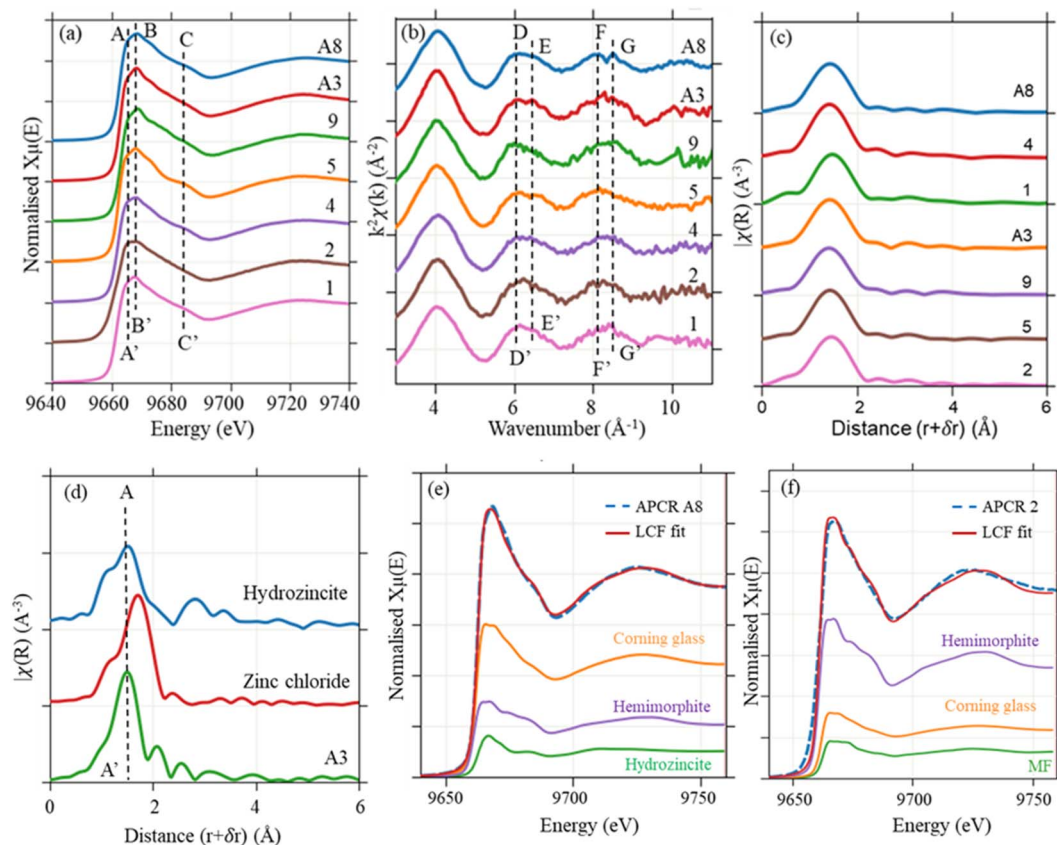


Fig. 5 (a) Zn K-edge XANES spectra of raw APCRs; (b) Zn K-edge EXAFS spectra of raw APCRs; (c and d) Fourier transform of the EXAFS spectra; (e and f) linear combination fitting of APCR 9 and 2, respectively.



**Table 4** Principal component analysis of Zn K-edge XANES of raw APCRs

Component	Eigenvalue	Variance	Cumulative variance	IND
1	82.90	0.938	0.938	0.04025
2	3.31	0.037	0.975	0.02301
3	1.17	0.013	0.988	0.01662
4	0.40	0.004	0.993	0.02229
5	0.25	0.002	0.996	0.04242
6	0.20	0.002	0.998	0.12690
7	0.13	0.001	1.0	NA

**Table 5** Target transformation of potential phases from Zn K-edge XANES

Phase	Chi square	R Value	Spoil
ZnCl <sub>2</sub>	0.69760	0.00068	0.9185
Corning glass IR-X	0.14646	0.00014	1.3122
Hemimorphite	0.50872	0.00054	1.6640
Hydrozincite	1.74022	0.00164	2.1260
Hopeite	1.13807	0.00117	2.5550
Willemite	0.86481	0.00093	3.7450
MF	0.45643	0.00045	3.9522
Franklinite	1.97155	0.00165	4.0789

–0.034 Å; Debye–Waller factor = 0.005; R-factor = 0.009). The fit results of APCR A3 with ZnCl<sub>2</sub> have a significantly higher R-factor of 0.042, approximately three times larger than obtained

with ZnO, indicating a poor fit result. Zn in APCR A3 is, therefore, predominantly tetrahedrally coordinated with oxygen atoms, rather than with chloride atoms.

#### 4.4 Zinc speciation in the “pH 9” and leached air pollution control residues

The Zn K-edge XANES spectra of raw APCRs A8, 9 and 1 can be compared with those of the same APCRs neutralised to a target pH of 9 in Fig. 7a (without separation of a leachate). The increased prominence of the features labelled A, B and C in the “pH 9” APCRs indicates changes in speciation. Differences in the white line regions of the “pH 9” APCRs also reveal differences in phase composition. The Zn K-edge spectra of the “pH 9” samples do not show any resemblance to zinc chloride or oxychloride, despite a large amount of chloride in the system from the APCR itself and the addition of HCl. Normal probability plots of the mineral proportions determined by LCF in the “pH 9” APCRs along with the raw APCRs show a significantly increased proportion of hydrozincite (Fig. 6, inset). The proportions of hemimorphite (particularly), spinel and glass, are lower in the “pH 9” than raw samples, although the difference is not statistically evidenced (Fig. A5, SI Appendix A), suggest that these poorly crystalline species have been altered to hydrozincite.

Zn K-edge XANES spectra of APCR A8 after leaching with water at an unadjusted pH of 11.84, and after leaching with diluted HNO<sub>3</sub> at pH 9.57 (both after leachate separation) are also shown in Fig. 7a. These spectra can be observed to be very

**Table 6** Mineral proportions determined by linear combination fitting of Zn K-edge XANES spectra of APCRs

APCR	APCR spinel (MF)	Hemimorphite (Zn <sub>4</sub> Si <sub>2</sub> O <sub>7</sub> (OH) <sub>2</sub> ·H <sub>2</sub> O)	Corning glass IR-X	Hopeite (Zn <sub>3</sub> (PO <sub>4</sub> ) <sub>2</sub> ·xH <sub>2</sub> O)	Hydrozincite (Zn <sub>5</sub> (CO <sub>3</sub> ) <sub>2</sub> (OH) <sub>6</sub> )	R-Factor
<b>(a) Raw APCRs</b>						
1		0.72		0.03	0.25	0.0003
2	0.14	0.61	0.25			0.0030
4	0.32		0.32	0.35		0.0004
5	0.61		0.16		0.23	0.0029
A8		0.29	0.6		0.13	0.00014
9	0.32	0.64			0.04	0.00012
Average*	0.35	0.57	0.33	0.19	0.16	
Standard deviation*	0.19	0.19	0.19	0.23	0.10	
<b>(b) Subsamples of APCR A3</b>						
A3i	0.35			0.55	0.1	0.0017
A3ii	0.39	0.36			0.25	0.00038
A3iii	0.48		0.24		0.28	0.0022
A3iv			0.87		0.13	0.0005
A3v	0.49		0.17		0.34	0.0018
Average	0.38	0.37	0.36	0.32	0.19	
Standard deviation	0.11	0.19	0.29	0.20	0.10	
<b>(c) pH 9 APCRs</b>						
1		0.15		0.3	0.56	0.0080
A8		0.09	0.33		0.58	0.0040
9	0.16	0.32			0.52	0.00014
Average	0.16	0.19	0.33	0.30	0.55	
Standard deviation	NA	0.12	NA	NA	0.03	
Overall average	0.37	0.36	0.37	0.31	0.31	
Overall std dev.	0.16	0.23	0.25	0.21	0.17	



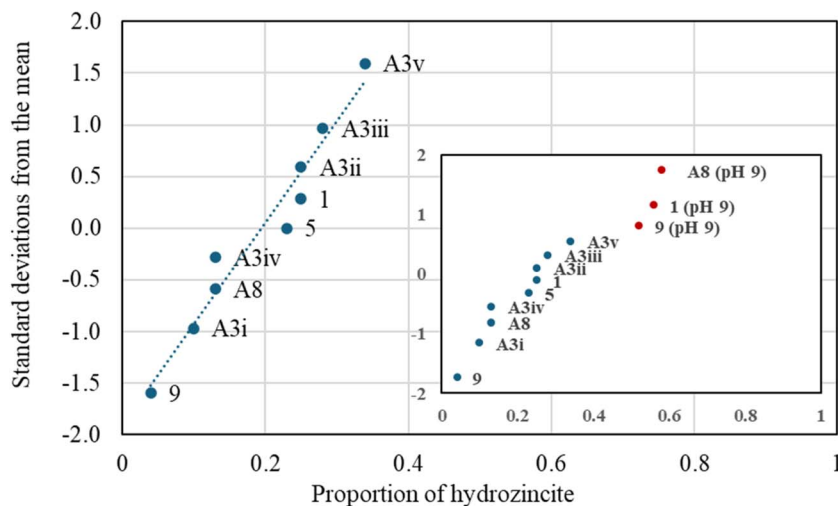


Fig. 6 The linear cumulative normal probability plot of hydrozincite proportions in all raw APCR samples containing hydrozincite (main) indicates that they belong to the same population. The inset shows significantly increased proportions of hydrozincite in APCRs neutralised to a target pH of 9.

similar to those of the “pH 9” APCRs. Zn K-edge EXAFS spectra of the same samples and their Fourier transform spectra are present in Fig. 7c and d, and the observation is consistent with the XANES result. A comparison of the Zn K-edge XANES spectrum of leached APCR A8 at pH 9.57 with that of hydrozincite (Fig. 7b) shows a very strong resemblance, and the LCF results indicate that the sample is 88% hydrozincite and 12% hemimorphite. The best LCF fit of Zn K-edge XANES spectrum for APCR A8 (pH 9.57) in the presence of zinc chloride, yielded a poor fit (Fig. A10, SI Appendix A), indicating that only a very minor amount of zinc chloride is present in the sample.

Curve fitting to theoretical standards was performed to fit theoretical spectra (*i.e.*, ZnO with tetrahedral Zn–O and ZnCl<sub>2</sub> with tetrahedral Zn–Cl), respectively, to the experimental one of raw APCR A8 pH 9.57, shown in Fig. A11 and A12, SI Appendix A. The best fit results (Table A1 and Fig. A11a, b, SI Appendix A) show that the first shell of APCR A8 pH 9.57 was obtained with a coordination number of 5.1 at a distance of 2.012 Å ( $S_0^2 = 0.93$ ;  $E_0 = 2.36$  eV;  $\Delta R = 0.048$  Å; Debye–Waller factor = 0.012;  $R$ -factor = 0.014). The fit results of APCR A8 pH 9.57 with ZnCl<sub>2</sub> have a significantly higher  $R$ -factor of 0.120, approximately nine times larger than obtained with ZnO, indicating a poor fit result. Zn in APCR A8 pH 9.57 is, therefore, predominantly coordinated with oxygen atoms, rather than with chloride atoms.

#### 4.5 Zinc leaching from raw and “pH 9” APCRs

Zn leachability from the raw APCRs in BS EN 12457-2:2002 (ref. 34) and DD CEN/TS 15364:200,<sup>35</sup> and “pH 9” APCRs A3, 4 and 5 in BS EN 12457-2:2002, has been plotted as a function of pH in Fig. 8; 1 mg kg<sup>-1</sup> leached from the solid equates to 1.5 mM. The pHs of the water-based leachates ranged from 11.83–12.36 for the raw APCRs, and the actual pHs of the “pH 9” APCRs ranged from 10.0–10.7 as the samples continued to react following initial adjustment to the target pH of 9 with HCl. The “pH 9” APCRs dis-agglomerated when immersed for leaching, and the

leachate concentrations for the raw APCRs and “pH 9” APCRs fall along the same curve in Fig. 8.

Table 7 presents saturation indices calculated using PHREEQC for candidate solid phases that may have controlled the observed leachate concentrations in the pH-dependent leaching of raw APCR A3. The main contributors to the charge balance were Ca<sup>2+</sup>, Na<sup>+</sup>, K<sup>+</sup>, Cl<sup>-</sup> and SO<sub>4</sub><sup>2-</sup>. A small shortage of anions (2–5%) is likely to be carbonate ion in this pH range. The phases with saturation indices closest to 0 at alkaline pH were Zn(OH)<sub>2</sub>, or possibly ZnO, and it therefore seems likely that these phases controlled the concentrations of Zn in the leachate by precipitation. These results are consistent with the findings of previous workers in Table 1. Interestingly, at pH 9.57, the present work also shows possible control of the leachate concentration by Zn<sub>5</sub>(OH)<sub>8</sub>Cl, which was also determined by Zhang *et al.*<sup>10</sup> at pH ~ 8, or Zn<sub>5</sub>(CO<sub>3</sub>)<sub>2</sub>(OH)<sub>6</sub>, and is consistent with our XAS findings regarding Zn speciation in the solid.

## 5 Discussion

### 5.1 Raw air pollution control residues

The results of PCA and LCF of Zn K edge XANES (Table 6) show several phases present in the raw APCRs in significant and varying proportions: (i) a spinel phase, (ii) a glassy or crystalline silicate phase; (iii) a phosphate phase, and (iv) hydrozincite. All Zn–K edge APCR EXAFS spectra are dominated by a single strong oscillation, which is consistent with poor crystallinity of the identified phases, and presence of Zn in solid solution and glass. This oscillation matches the Zn–O shell better than the Zn–Cl shell, indicating that Zn chlorides can be present in only a very minor amounts. This finding contrasts with those of other researchers (Table 1).

Fe K-edge XANES showed that Fe in the raw APCRs is distributed between magnetite and ferrihydrite, in variable proportions from 0 to 100%. Enrichment of Zn, Cu, Ti, Ni, Mn



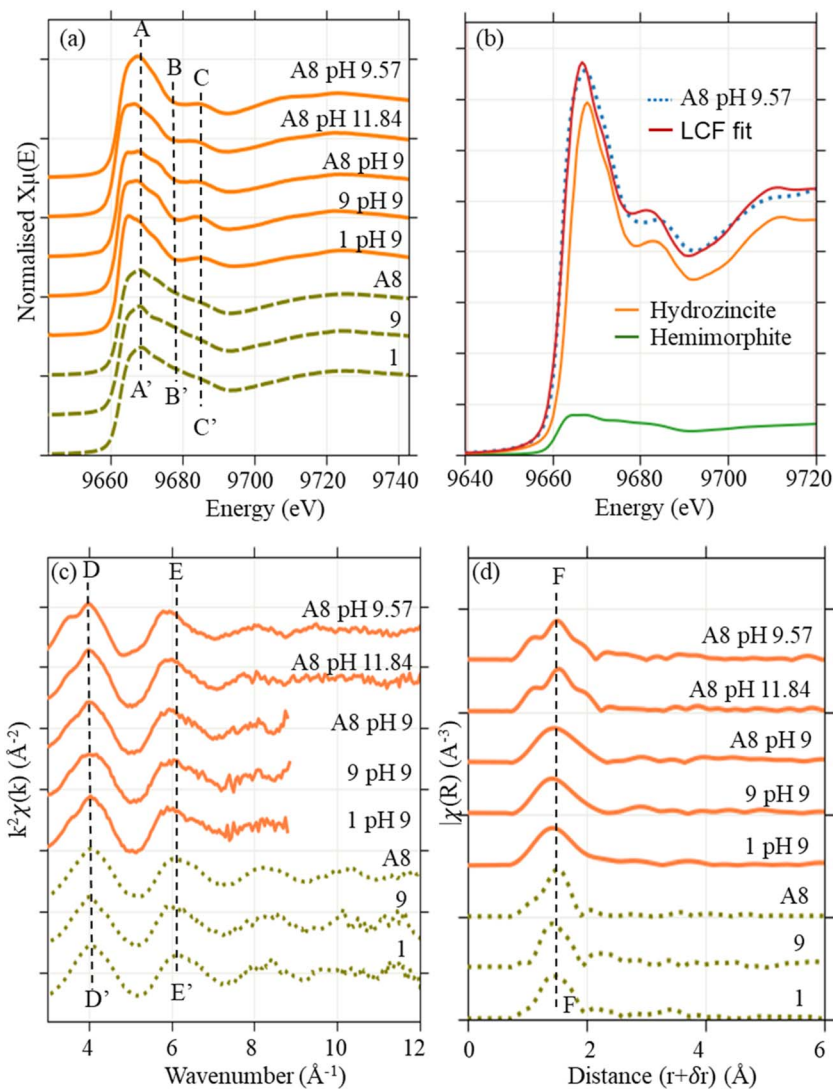


Fig. 7 (a) Zn K-edge X-ray XANES spectra for raw APCRs 1, 9 and A8, compared with the “pH 9” APCRs after partial neutralisation with HCl (without leachate separation), as well as APCR 8 after leaching with water at unadjusted pH 11.84, and diluted  $\text{HNO}_3$  at pH 9.57 (after leachate separation); (b) comparison of the latter spectrum with hydrozincite, and the linear combination fit based on hydrozincite and hemimorphite; (c) Zn K-edge EXAFS spectra for raw APCRs; and (d) in Fourier transform of the EXAFS spectra (uncorrected for phase shift), with an interval  $k = 3\text{--}8.7 \text{ \AA}^{-1}$  for A8 pH 9, 9 pH 9 and 1 pH 9, and  $k = 3\text{--}12 \text{ \AA}^{-1}$  for the remaining raw APCRs and a Hanning window.

and Cr in the magnetic fraction compared to the raw APCR is consistent with findings by De Boom, *et al.*<sup>47</sup> for MSW incinerator ashes, and Wang<sup>48</sup> and Kukier, *et al.*<sup>49</sup> for the magnetic fraction of coal fly ash. While Zn K-edge XANES and EXAFS of the magnetic fraction of UK APCR show a structure most similar to that of magnetite, there is also a resemblance to franklinite, which was identified in APCRs by others<sup>6,14,21</sup>. Yu, *et al.*<sup>17</sup> did not include franklinite in their fit, but speculated that fit would be improved by its inclusion. Zn K-edge XANES for Swedish MSW incinerator ashes and APCRs clearly indicates the presence of franklinite.<sup>6,21</sup> Our study of the magnetic fraction of APCR clearly shows the presence of a zinc-substituted magnetite, for which an identical reference material would be difficult to obtain. The absence of more than one main oscillation in the Zn K edge EXAFS spectrum of APCR (Fig. 4) also suggests that Zn is

not sorbed to ferrihydrate,<sup>50</sup> though sorbed Zn has been identified by others.<sup>6</sup>

Both hemimorphite ( $\text{Zn}_4\text{Si}_2\text{O}_7(\text{OH})_2 \cdot \text{H}_2\text{O}$ ) and willemite ( $\text{Zn}_2\text{SiO}_4$ ), are common in nature, where they may be found with hydrozincite<sup>51</sup> and also in mining and metallurgical wastes.<sup>32,52</sup> Hemimorphite can be formed from a variety of precursors at relatively low temperature;<sup>53</sup> it dehydrates to willemite at 364–912 °C,<sup>54</sup> which decomposes to ZnO and SiO<sub>2</sub> at temperatures unlikely to be encountered in EfW facilities (~1500 °C<sup>55</sup>). Hemimorphite in the APCRs could therefore only form in the fabric filter. Predominance information for hemimorphite over ZnCl<sub>2</sub> in the conditions that prevail in APCRs is not available, but willemite predominates over ZnCl<sub>2</sub> under alkaline conditions in aqueous systems at ambient temperature and open to the atmosphere.<sup>56</sup> Astrup, *et al.*<sup>8</sup> suggested that willemite also



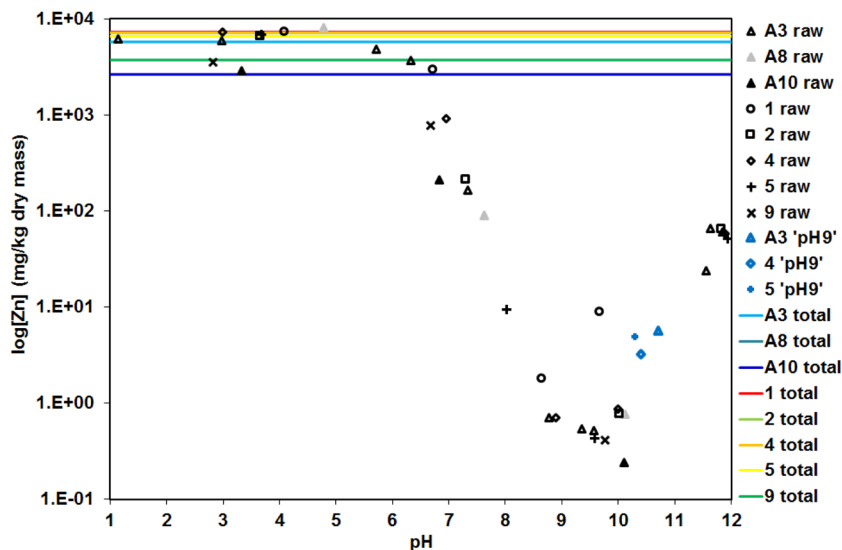


Fig. 8 Zn leachability from seven APCRs as a function of pH compared with total Zn concentrations (BS EN 12457-2:2002 and DD CEN/TS 15364:2006 results for raw APCRs, and BS EN 12457-2:2002 results for pH 9 APCRs).

contributed to control of Zn leachability for some APCRs, but this is unlikely in our APCRs, since it was not identified as a main Zn-containing phase in the raw APCR and would not form during the leaching process. Given supersaturation of our leachates with compounds with larger solubility product constants, control of Zn leachability by willemite ( $K_{sp} = 10^{-15.33}$  (ref. 36)) is unlikely. Si was below the detection limit in our leachates, so neither hemimorphite nor willemite could be included in our modelling. Hemimorphite may control Zn leaching at mildly acidic pH, though it is likely to convert to hydrozincite at low alkaline pH.<sup>57</sup>

Apatite ( $\text{Ca}_5(\text{PO}_4)_3\text{OH}$ ) is the most common phosphate mineral on Earth. It forms a wide-ranging solid solution, with Ca being easily replaced by Na, K and other elements including Zn. Zinc phosphate was found by Pattanaik and Huggins<sup>58</sup> in oil fly ash. Several researchers have found that the addition of a phosphate

source to different kinds of waste increased retention of zinc, with identification of both  $\text{Zn}_3(\text{PO}_4)_2$  (ref. 59) and apatite.<sup>60–62</sup> The amount of P in these UK APCRs ranges from 0.20 to 0.59%. The presence of a phosphate phase containing zinc is thus likely. While the Zn K-edge spectrum for hopeite,  $\text{Zn}_3(\text{PO}_4)_2 \cdot \text{H}_2\text{O}$ , contributed to good LCF fits for the Zn K-edge spectra of many of the raw APCRs, there is a similarity between the XANES and EXAFS spectra of apatite,<sup>63</sup> so the presence of apatite is also a possibility. Given the many possible compositions of apatite, a reference material with an exactly matching spectrum to any or all of the APCRs would be hard to find.

At the  $\text{CO}_2$  partial pressures in EfW flue gas ( $\sim 0.1$ ), hydrozincite ( $\text{Zn}_5(\text{CO}_3)_2(\text{OH})_6$ ) is stable only between about 100 °C and 150 °C.<sup>54</sup> This suggests that the hydrozincite in APCRs is formed during cooling, *i.e.*, in the fabric filter. Recent research by Rissler *et al.*<sup>6</sup> also found hydrozincite, and its absence in the

Table 7 Saturation indices for the pH-dependent leaching of APCR A3 according to DD CEN/TS 15364:2006<sup>a</sup>

Species	Leachate pH					
	2.98	5.72	8.77	9.57	11.55	11.84*
Zincite ( $\text{ZnO}$ )	—	−2.7	−0.72	0.72	0.98	1.1
$\text{Zn}(\text{OH})_2$	—	−3.3	−1.3	0.1	0.37	0.47
$\text{Zn}_2(\text{OH})_3\text{Cl}$	—	−4.6	−3.7	−1.7	−3.1	−3.7
Simonkolleite ( $\text{Zn}_5(\text{OH})_8\text{Cl}$ )	—	—	—	0.44	−2.2	−2.2
$\text{ZnCO}_3 \cdot \text{H}_2\text{O}$	—	—	−3.2	−3.3	—	—
Smithsonite ( $\text{ZnCO}_3$ )	—	—	−3.4	−3.6	—	—
Hydrozincite ( $\text{Zn}_5(\text{CO}_3)_2(\text{OH})_6$ )	—	—	−4.6	−0.6	−4.8	−4.7
Willemite ( $\text{Zn}_2\text{SiO}_4$ )	—	−3.9	2.5	—	—	—
$\text{ZnSiO}_3$	−1.5	−2.0	2.5	4.7	4.1	4.1
Franklinite ( $\text{ZnFe}_2\text{O}_4$ )	—	—	—	—	—	—

<sup>a</sup> Solid phases likely to control solution concentrations ( $-1 < \text{saturation index} < 1$ ). \* Water leachate. “—” indicates phases highly unlikely to control solution concentrations with  $5 < \text{saturation index} < -5$ .



findings of previous workers may relate to other operating conditions, *e.g.*, use of electrostatic precipitators that operate at a higher temperature in older plants. Modern operating conditions emphasise a rapid transition from very high operating temperatures (>850 °C) to ambient temperature, to avoid dioxin formation. This temperature regime may also avoid formation of ZnO and ZnCl<sub>2</sub>. Hydrozincite predominates over ZnCO<sub>3</sub> or Zn(OH)<sub>2</sub> at pH greater than 7.2 in aqueous systems at ambient temperature and open to the atmosphere,<sup>64</sup> *i.e.*, the environment of the raw, “pH 9” and leached APCRs.

## 5.2 “pH 9” APCRs

Zn K-edge XANES showed convincing evidence of formation of hydrozincite in the “pH 9” APCRs treated by partial neutralisation with HCl. Decreased proportions of hemimorphite, spinel and glass in the “pH 9” APCRs compared to the raw samples suggest that the poorly crystalline forms of all of these species have been altered to hydrozincite. However, observation of increased hydrozincite also in the leached APCRs at pH 11.82 and 9.57 suggests that the presence of water to enable dissolution of soluble phases from the raw APCRs is more important for formation of secondary hydrozincite than the partial neutralisation reaction.

Agglomeration of APCRs as a result of partial neutralisation with concentrated acid is sometimes reported in industrial practice at full-scale. It seems to be caused by formation of secondary phases. Since typical industrial methods and contact times are as unlikely to achieve a stable pH of 9 in acid blending as the “pH 9” APCRs produced in our laboratory, which had final pHs from 10.0–10.7, it is possible that the agglomerating phases could include small amounts of thaumasite or calcium silicate hydrate. Substitution of Zn for Ca in the related mineral ettringite (Ca<sub>6</sub>Al<sub>2</sub>(SO<sub>4</sub>)<sub>3</sub>(OH)<sub>12</sub>·26H<sub>2</sub>O) has been postulated,<sup>65</sup> but the evidence is weak.

Regardless of these potential agglomeration reactions, the fact that Zn leaching data from the raw APCRs and “pH 9” APCRs fall along the same curve in Fig. 8 clearly demonstrates that the treatment with concentrated acid does not change the mechanisms that control Zn leachability. Although Zn leachability is decreased by partial neutralisation to pH 10–10.7 (and would be further decreased if a stable pH of 9 could be achieved), this pH is unlikely to prevail in contact with landfill leachate with a typical pH of 5–8. In general, partial neutralisation cannot be considered as a long-term strategy to avoid environmental risk, as a mildly alkaline pH will be neutralised by carbonation and acidification, through interaction with the atmosphere and groundwater.

In the context of assessment of the environmental risks associated with APCRs, our findings should be considered in the context of the toxicity, leachability and bioavailability of the identified Zn phases, whereby our results suggested control of Zn leaching by precipitation of zinc hydroxide, and possibly by dissolution of hydrozincite at intermediate alkaline pH. Molina, *et al.*<sup>66</sup> have found the following sequence of bioavailability: hydrozincite > hemimorphite > zincite ≈ smithsonite ≫ sphaalerite.

## 6 Conclusions

Zn K-edge XAS studies of magnetic and non-magnetic fractions, supplemented by Fe K-edge XAS, provided a better insight into the speciation of zinc in APCRs, showing that magnetite can be an important repository of zinc and that hemimorphite, glass and zinc phosphate are important Zn-containing phases, along with hydrozincite. The magnetite phase can also incorporate other potential pollutants, including Cu, Ni and Cr. Leaching studies show that with or without treatment by partial neutralisation, the mineral controls on zinc leaching behaviour are the same.

## Author contributions

Amitava Roy: methodology, formal analysis, investigation, resources, data curation, writing, visualization, funding acquisition. Dan Ting Chen: methodology, formal analysis, investigation, writing, visualization. Anna Bogush: methodology, formal analysis, investigation. Julia A. Stegemann: conceptualisation, methodology, formal analysis, resources, writing, visualisation, supervision, project administration, funding acquisition.

## Conflicts of interest

All the authors declare no conflict of interest, either financial or otherwise.

## Abbreviations

EfW	Energy from waste
MSW	Municipal solid waste
APCR	Air pollution control residue
XRD	X-ray powder diffraction
XANES	X-ray absorption near edge structure
EXAFS	Extended X-ray absorption fine structure
CAMD	J. Bennett Johnston, Sr, Center for Advanced Microstructures and Devices
ICP OES/MS	Inductively coupled plasma optical emission spectrometry/mass spectrometry
PCA	Principal component analysis
UCL	University College London
XAS	X-ray absorption spectroscopy

## Data availability

The data supporting this article have been included in the supplementary information (SI). Supplementary information is available. See DOI: <https://doi.org/10.1039/d5em00651a>.

## Acknowledgements

We would like to thank: Paul Fernee and Peter Chesney (Environment Agency) for samples; Kym Jarvis (NERC ICP facility);



Judith Zhou and Ian Sturtevant (UCL CEGE laboratory); and the Smithsonian National Museum of Natural History, for the glass standard. This work was funded by the Environment Agency, UCL CEGE, CAMD, the UK EPSRC (Grant EP/M00337X/1) and the Louisiana Board of Regents (LEQSF(2016-17)-ENH-TR-07).

## References

- 1 A. Bogush, J. A. Stegemann, I. Wood and A. Roy, Element composition and mineralogical characterisation of air pollution control residue from UK energy-from-waste facilities, *Waste Manage.*, 2015, **36**, 119.
- 2 L. S. Morf, P. H. Brunner and S. Spaun, Effect of operating conditions and input variations on the partitioning of metals in a municipal solid waste incinerator, *Waste Manage. Res.*, 2000, **18**, 4–15.
- 3 A. Jakob, S. Stucki and P. Kuhn, Evaporation of heavy metals during the heat treatment of municipal solid waste incinerator fly ash, *Environ. Sci. Technol.*, 1995, **29**, 2429–2436.
- 4 W. Seeker, W. Lanier and M. Heap, *Municipal Waste Combustion Study: Combustion Control of Organic Emissions*, EPA, Research Triangle Park, NC, 1987.
- 5 B. J. Stuart and D. S. Kosson, Characterization of municipal waste combustion air pollution control residues as a function of particle size, *Combust. Sci. Technol.*, 1994, **101**, 527–548.
- 6 J. Rissler, K. K. Fedje, K. Klementiev, B. Ebin, C. Nilsson, H. M. Rui, T. M. Kluffhaugen, S. Sala and I. Johansson, Zinc speciation in fly ash from MSWI using XAS-novel insights and implications, *J. Hazard. Mater.*, 2024, **477**, 135203.
- 7 T. T. Eighmy, J. D. Eusden, J. E. Krzanowski, D. S. Domingo, D. Staempfli, J. R. Martin and P. M. Erickson, Comprehensive approach toward understanding element speciation and leaching behavior in municipal solid waste incineration electrostatic precipitator ash, *Environ. Sci. Technol.*, 1995, **29**, 629–646.
- 8 T. Astrup, J. J. Dijkstra, R. N. Comans, H. A. Van der Sloot and T. H. Christensen, Geochemical modeling of leaching from MSWI air-pollution-control residues, *Environ. Sci. Technol.*, 2006, **40**, 3551–3557.
- 9 L. Wang, Q. Chen, I. A. Jamro, R. Li, Y. Li, S. Li and J. Luan, Geochemical modeling and assessment of leaching from carbonated municipal solid waste incinerator (MSWI) fly ash, *Environ. Sci. Pollut. Res.*, 2016, **23**, 12107–12119.
- 10 H. Zhang, P.-j. He, L.-m. Shao, J.-h. Feng and Q.-k. Cao, Leaching behavior of Pb and Zn in air pollution control residues and their modeling prediction, *J. Environ. Sci.*, 2006, **18**, 583–586.
- 11 L. Le Forestier and G. Libourel, Characterization of flue gas residues from municipal solid waste combustors, *Environ. Sci. Technol.*, 1998, **32**, 2250–2256.
- 12 P. Fermo, F. Cariati, A. Pozzi, M. Tettamanti, E. Collina and D. Pitea, Analytical characterization of municipal solid waste incinerator fly ash: Part II, *Fresen. J. Anal. Chem.*, 2000, **366**, 267–272.
- 13 R. P. Struis, C. Ludwig, H. Lutz and A. M. Scheidegger, Speciation of zinc in municipal solid waste incineration fly ash after heat treatment: an X-ray absorption spectroscopy study, *Environ. Sci. Technol.*, 2004, **38**, 3760–3767.
- 14 M. Takaoka, T. Yamamoto, T. Tanaka, N. Takeda, K. Oshita and T. Uruga, Direct speciation of lead, zinc and antimony in fly ash from waste treatment facilities by XAFS spectroscopy, *Phys. Scr.*, 2005, **2005**, 943.
- 15 J. Hyks, T. Astrup and T. H. Christensen, Influence of test conditions on solubility controlled leaching predictions from air-pollution-control residues, *Waste Manage. Res.*, 2007, **25**, 457–466.
- 16 M. J. Quina, J. C. Bordado and R. M. Quinta-Ferreira, Treatment and use of air pollution control residues from MSW incineration: An overview, *Waste Manage.*, 2008, **28**, 2097–2121.
- 17 M. Yu, S. Tian, W. Chu, D. Chen, Q. Wang and Z. Wu, Speciation of zinc in secondary fly ashes of municipal solid waste at high temperatures, *Synchrotron Radiat.*, 2009, **16**, 528–532.
- 18 A. P. Bayuseno and W. W. Schmahl, Characterization of MSWI fly ash through mineralogy and water extraction, *Resour. Conserv. Recycl.*, 2011, **55**, 524–534.
- 19 Y.-M. Zhu, H. Zhang, S.-S. Fan, S.-J. Wang, Y. Xia, L.-M. Shao and P.-J. He, In-situ determination of metallic variation and multi-association in single particles by combining synchrotron microprobe, sequential chemical extraction and multivariate statistical analysis, *J. Hazard. Mater.*, 2014, **276**, 241–252.
- 20 X. Bolaños Chamorro, B. Ayati and D. Newport, *Chemical Characterisation and Leaching Properties of Air Pollution Control Residues (APCr) from Municipal Solid Waste Incineration (MSWI) Sites in the UK*, 2023.
- 21 J. Rissler, K. Klementiev, J. Dahl, B.-M. Steenari and M. Edo, Identification and quantification of chemical forms of Cu and Zn in MSWI ashes using XANES, *Energy Fuels*, 2020, **34**, 14505–14514.
- 22 C. Biagioni and M. Pasero, The systematics of the spinel-type minerals: An overview, *Am. Mineral.*, 2014, **99**, 1254–1264.
- 23 A. V. Carvalho and C. B. Sclar, Experimental determination of the ZnFe<sub>2</sub>O<sub>4</sub>-ZnAl<sub>2</sub>O<sub>4</sub> miscibility gap with application to franklinite-gahnite exsolution intergrowths from the Sterling Hill zinc deposit, New Jersey, *Econ. Geol.*, 1988, **83**, 1447–1452.
- 24 C. Frondel and C. Klein Jr, Exsolution in franklinite, *Am. Mineral.*, 1965, **50**, 1670–1680.
- 25 Y. Wei, T. Shimaoka, A. Saffarzadeh and F. Takahashi, Mineralogical characterization of municipal solid waste incineration bottom ash with an emphasis on heavy metal-bearing phases, *J. Hazard. Mater.*, 2011, **187**, 534–543.
- 26 R. Helmuth, *Fly Ash in Cement and Concrete*, 1987.
- 27 R. T. Hemmings and E. E. Berry, Speciation in size and density fractionated fly ash, *MRS Online Proc. Libr.*, 1985, **65**, 91.
- 28 S. Gomes, M. François, M. Abdelmoula, P. Refait, C. Pellissier and O. Evrard, Characterization of magnetite in silico-aluminous fly ash by SEM, TEM, XRD, magnetic



- susceptibility, and Mössbauer spectroscopy, *Cem. Concr. Res.*, 1999, **29**, 1705–1711.
- 29 J. A. Stegemann, A. Roy, R. J. Caldwell, P. J. Schilling and R. Tittsworth, Understanding environmental leachability of electric arc furnace dust, *J. Environ. Eng.*, 2000, **126**, 112–120.
- 30 T. Suetens, M. Guo, K. Van Acker and B. Blanpain, Formation of the ZnFe<sub>2</sub>O<sub>4</sub> phase in an electric arc furnace off-gas treatment system, *J. Hazard Mater.*, 2015, **287**, 180–187.
- 31 N. M. Piatak, M. B. Parsons and R. R. Seal II, Characteristics and environmental aspects of slag: A review, *Appl. Geochem.*, 2015, **57**, 236–266.
- 32 A. Manceau, B. Lanson, M. L. Schlegel, J. C. Harge, M. Musso, L. Eybert-Berard, J.-L. Hazemann, D. Chateigner and G. M. Lamble, Quantitative Zn speciation in smelter-contaminated soils by EXAFS spectroscopy, *Am. J. Sci.*, 2000, **300**, 289–343.
- 33 P. G. Jeffery, D. Hutchison and P. Jeffrey, *Chemical Methods of Rock Analysis*, Elsevier, 1981.
- 34 British Standards Institution, *BS EN 12457-2:2002, Characterisation of waste - Leaching, Compliance test for leaching of granular waste materials and sludges*, British Standard, UK, 2002.
- 35 British Standard Institution, *BS DS CEN/TS 15364:2006, Characterization of waste - Leaching behaviour tests - Acid and base neutralization capacity test*, British Standard, UK, 2006.
- 36 D. L. Parkhurst and C. Appelo, Description of input and examples for PHREEQC version 3—a computer program for speciation, batch-reaction, one-dimensional transport, and inverse geochemical calculations, *US Geological Survey Techniques and Methods*, 2013, vol. 6, p. 497.
- 37 W. Preis and H. Gamsjäger, (Solid+ solute) phase equilibria in aqueous solution. XIII. Thermodynamic properties of hydrozincite and predominance diagrams for (Zn<sup>2+</sup>+ H<sub>2</sub>O+ CO<sub>2</sub>), *J. Chem. Therm.*, 2001, **33**, 803–819.
- 38 B. C. Craft, A. M. Findley, G. L. Findley, S. P. McGlynn, J. D. Scott and F. H. Watson, LSU Center for Advanced Microstructures and Devices, *Rev. Sci. Instrum.*, 1989, **60**, 7.
- 39 M. Newville, Larch: an analysis package for XAFS and related spectroscopies, *J. Phys.: Conf. Ser.*, 2013, **430**, 012007.
- 40 B. Ravel and M. Newville, ATHENA, ARTEMIS, HEPHAESTUS: data analysis for X-ray absorption spectroscopy using IFEFFIT, *Synchrotron Radiat.*, 2005, **12**, 537–541.
- 41 S. M. Webb, SIXpack: a graphical user interface for XAS analysis using IFEFFIT, *Phys. Scri.*, 2005, **2005**, 1011.
- 42 S. Calvin, *XAFS for Everyone*, CRC press, 2024.
- 43 E. R. Malinowski and D. G. Howery, *Factor Analysis in Chemistry*, Wiley, New York, 2002.
- 44 E. R. Malinowski, Theory of error for target factor analysis with applications to mass spectrometry and nuclear magnetic resonance spectrometry, *Anal. Chim. Acta*, 1978, **103**, 339–354.
- 45 M. Alfeld, V. Gonzalez and A. van Loon, Data intrinsic correction for working distance variations in MA-XRF of historical paintings based on the Ar signal, *X Ray Spectrom.*, 2021, **50**, 351–357.
- 46 D. T. Chen, Speciation of Toxic Pollutants in Hazardous Industrial Wastes by X-ray Absorption Spectroscopy, Doctoral dissertation, UCL (University College London), 2024.
- 47 A. De Boom, M. Degrez, P. Hubaux and C. Lucion, MSWI boiler fly ashes: Magnetic separation for material recovery, *Waste Manage.*, 2011, **31**, 1505–1513.
- 48 X. S. Wang, Mineralogical and chemical composition of magnetic fly ash fraction, *Environ. Earth Sci.*, 2014, **71**, 1673–1681.
- 49 U. Kukier, C. F. Ishak, M. E. Sumner and W. P. Miller, Composition and element solubility of magnetic and non-magnetic fly ash fractions, *Environ. Pollut.*, 2003, **123**, 255–266.
- 50 M. Nachtegaal and D. L. Sparks, Effect of iron oxide coatings on zinc sorption mechanisms at the clay-mineral/water interface, *J. Colloid Interface Sci.*, 2004, **276**, 13–23.
- 51 V. Coppola, M. Boni, H. A. Gilg, G. Balassone and L. Dejonghe, The “calamine” nonsulfide Zn–Pb deposits of Belgium: petrographical, mineralogical and geochemical characterization, *Ore Geol. Rev.*, 2008, **33**, 187–210.
- 52 P. Iavazzo, P. Adamo, M. Boni, S. Hillier and M. Zampella, Mineralogy and chemical forms of lead and zinc in abandoned mine wastes and soils: an example from Morocco, *J. Geochem. Explor.*, 2012, **113**, 56–67.
- 53 J. Yang, Y. Sun, Z. Chen and X. Zhao, Hydrothermal synthesis and optical properties of zinc silicate hierarchical superstructures, *Mater. Lett.*, 2011, **65**, 3030–3033.
- 54 Z. Ding, Z. Yin, H. Hu and Q. Chen, Comparison of thermal property and dissolution behavior of synthetic compound and natural hemimorphite, *Thermochim. Acta*, 2010, **511**, 168–173.
- 55 M. Takesue, H. Hayashi and R. L. Smith Jr, Thermal and chemical methods for producing zinc silicate (willemite): a review, *Prog. Cryst. Growth Char. Mater.*, 2009, **55**, 98–124.
- 56 J. I. Brugger, D. McPhail, M. Wallace and J. Waters, Formation of willemite in hydrothermal environments, *Econ. Geol.*, 2003, **98**, 819–835.
- 57 D. Medas, F. Podda, C. Meneghini and G. De Giudici, Stability of biological and inorganic hemimorphite: implications for hemimorphite precipitation in non-sulfide Zn deposits, *Ore Geol. Rev.*, 2017, **89**, 808–821.
- 58 S. Pattanaik and F. E. Huggins, Chemical nature of zinc in size fractionated particulate matter from residual oil combustion-A comparative study, *Atmos. Environ.*, 2020, **221**, 117099.
- 59 T. T. Eighmy, B. S. Crannell, J. E. Krzanowski, L. G. Butler, F. K. Cartledge, E. F. Emery, J. D. Eusden Jr, E. L. Shaw and C. A. Francis, Characterization and phosphate stabilization of dusts from the vitrification of MSW combustion residues, *Waste Manage.*, 1998, **18**, 513–524.
- 60 N. Basta, R. Gradwohl, K. Snethen and J. Schroder, Chemical immobilization of lead, zinc, and cadmium in smelter-



- contaminated soils using biosolids and rock phosphate, *J. Environ. Qual.*, 2001, **30**, 1222–1230.
- 61 D. Geysen, C. Vandecasteele, M. Jaspers, E. Brouwers and G. Wauters, Effect of improving flue gas cleaning on characteristics and immobilisation of APC residues from MSW incineration, *J. Hazard Mater.*, 2006, **128**, 27–38.
- 62 P. Piantone, F. Bodéan, R. Derie and G. Depelsenaire, Monitoring the stabilization of municipal solid waste incineration fly ash by phosphation: mineralogical and balance approach, *Waste Manage.*, 2003, **23**, 225–243.
- 63 Y. Tang, H. F. Chappell, M. T. Dove, R. J. Reeder and Y. J. Lee, Zinc incorporation into hydroxylapatite, *Biomaterials*, 2009, **30**, 2864–2872.
- 64 W. Preis and H. Gamsjäger, Thermodynamic investigation of phase equilibria in metal carbonate–water–carbon dioxide systems, *Chem. Mon.*, 2001, **132**, 1327–1346.
- 65 M. L. D. Gougar, B. E. Scheetz and D. D. Siemer, A novel waste form for disposal of spent-nuclear-fuel reprocessing waste: A vitrifiable cement, *Nucl. Technol.*, 1999, **125**, 93–103.
- 66 R. M. Molina, L. A. Schaidler, T. C. Donaghey, J. P. Shine and J. D. Brain, Mineralogy affects geoavailability, bioaccessibility and bioavailability of zinc, *Environ. Pollut.*, 2013, **182**, 217–224.

